Journal of Applied Research in Water and Wastewater
E-ISSN: 2476-6283
Journal homepage: https://arww.razi.ac.ir

Enhancement in performance and self-cleaning properties of PES membrane surface tailored by modified TiO_2

Mina Dolatshah[1], Ali Akbar Zinatizadeh[1,2,3*], Sirus Zinadini[1,2], Hadis Zangeneh[4], Shohreh Azizi[5,6], Mohamed Abdulgader[7,8], Malik Maaza[5,6]

[1]*Department of Applied Chemistry, Faculty of Chemistry, Razi University, Kermanshah, Iran.*
[2]*Environmental Pollution and Engineering Group, Environmental Research Center (ERC), Razi University, Kermanshah, Iran.*
[3]*Australian Centre for Water and Environmental Biotechnology (Formerly AWMC), The University of Queensland, Brisbane, Australia.*
[4]*Department of Chemical Engineering, Isfahan University of Technology, Isfahan, Iran.*
[5]*UNESCO-UNISA Africa Chair in Nanosciences and Nanotechnology, College of Graduate Studies, University of South Africa, Muckleneuk Ridge, Pretoria, South Africa.*
[6]*Nanosciences African Network (NANOAFNET), iThemba LABS-National Research Foundation, 1 Old Faure Road, Somerset West, Somerset West, Western Cape, South Africa.*
[7]*School of Engineering and Built Environment, Griffith University, Nathan Campus, QLD, Australia.*
[8]*Department of Environmental Science, Faculty of Environment and Natural Resources, Wadi Al-Shatti University, Libya.*

GRAPHICAL ABSTRACT

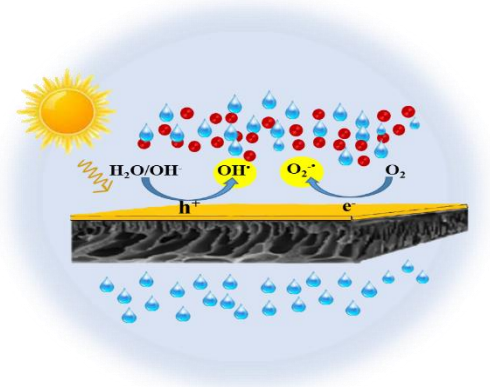

ARTICLE INFO

Article history:
Received 9 July 2022
Reviewed 12 October 2022
Received in revised form 14 November 2022
Accepted 15 November 2022
Available online 16 November 2022

Keywords:
PES membrane
TiO_2-based photocatalytic membrane
Nanofiltration
Antifouling
Self-cleaning

Article type: Research Article

ABSTRACT

In this study, the polyethersulfone (PES) membranes were established by surface modification using C, N codoped-TiO_2/WO_3 (LTW) photocatalytic nanocomposite to amelioration of the membrane performance in terms of antifouling and self-cleaning properties. The nanocomposite membranes were characterized by ATR-FTIR, SEM, AFM, and water contact angle (WCA). The photocatalytic membranes' performance was evaluated using assessment of the pure water flux (PWF), antifouling behavior, photoactivity, and long-term filtration. The membrane modification improved morphology and hydrophilicity of the membranes surface, contributing to the enhanced permeability (PWF of 49.65 kg/m^2.h), and substantial antifouling property (FRR of 96.96 %) as well as photoactivity (94.36 % dye removal) of the optimal photocatalytic membrane (M_3 membrane). The long-term filtration of the optimal membrane represented its high performance and noteworthy antifouling resistance.

1. Introduction

Nanofiltration Membrane technology has gained prominence in water and wastewater treatment over the last few decades as a result of its high separation efficiency and low energy consumption. In addition to the aforementioned advantages, a lack of (low) chemical additives or phase transitions, and low operating costs when compared to the prior treatment technologies have caused its further application (L. Wu et al.

*Corresponding author Email: zinatizadeh@gmail.com

How to cite: M. Dolatshah, A.A. Zinatizadeh, S. Zinadini, H. Zangeneh, S. Azizi, M. Abdulgader, M. Maaza, Enhancement in performance and self-cleaning properties of PES membrane surface tailored by modified TiO_2, *Journal of Applied Research in Water and Wastewater*, 9 (2), 2022, 147-153.

2018). Notwithstanding the great potential of the PES nanofiltration membranes in separation processes, membrane fouling seriously limits the application of membranes (Rahimi et al. 2021). The major elements in tailoring the permeate quality of filtration including hydrophilicity and its chemical selectivity are factors that can be controlled by membrane modification. Photocatalytic nanocomposites are a promising option to improve membrane performance (Chiao et al. 2020; Weiwei et al. 2018). The photocatalysts in addition to improving the membrane hydrophilicity, could also oxidize the pollutant molecules deposited on it (Zangeneh et al. 2019b). In this regards, a great efforts has been in progress via employing various photocatalysts, for instance titanium dioxide (TiO_2) (Rahimpour et al. 2008), graphene oxide (GO) (Mansourpanah et al. 2015), metal–organic frameworks (MOFs) (Pejman et al. 2021), carbon quantum dots (CQDs) (Chong et al. 2021), copper sulfide (CuS) (Zabihi et al 2020), and bismuth oxide (Bi_2O_3) (Zou et al. 2020). It has been proven that, The TiO2 semiconductor is an efficient photocatalyst for membranes modification with the goal of amelioration in permeation flux and antifouling properties as well as separation performance (Aboamera et al. 2018). However, the large band gap of TiO_2 (3.2 eV) limits its application (Chi et al. 2019). As a result, many studies have been dedicated to the chemical functionalization of TiO2 to performance enhancement through coupling materials (Basumatary et al. 2022) and/or doping elements (Hadis Zangeneh et al. 2022).

Using novel C, N co-doped-TiO_2/WO_3 nanophotocatalyst, we were capable of tailoring the filtration performance of PES photocatalytic membranes. The main objective of this study was to investigate the effect of the nanocomposite addition on the fabricated PES membranes for morphology, surface roughness, filtration performance, and photoactivity. Finally, the photoactivity capability of the optimum photocatalytic membrane was studied during long-term filtration under continuously visible light irradiation.

2. Materials and methods

2.1. Synthesis of the photocatalytic nanocomposite

The L-Lysine (1wt. %)-TiO_2/WO_3 (4 wt. %) (LTW) photocatalytic composite selected as optimal photocatalyst as a result of an independent research work submitted elsewhere, was synthesized via a sol-gel process as described in the following. Initially, to prepare 1 wt% amino acid solution, the required amount of L-Lysine amino acid (Merck-Germany) was dissolved in 25 mL of ethanol under stirring to prepare solution A. Meanwhile, 6 ml of tetrabutyl ortho-titanate (TBOT, Merck-Germany) was added to the 25 ml of ethanol (Merck-Germany, 99%) dropwise under continuous stirring. The aforesaid mixture was then vigorously mixed while 5 ml of acetic acid (Merck-Germany, 99.8%) was added drop by drop, yielding solution B. Then, solution B was added to solution A gradually by assisted-sonication approach during 1 h. Next, 50 ml of 1.5 g/l ammonium p-tungstate (ApT, Merck-Germany) solution (solution C) also was poured into the mentioned mixture dropwise while being violently agitated. The final product was aged in ambient condition for 48 h. Ultimately, the final solution was dried at 70°C and subsequently collected precipitate was calcined for 4 h at 500°C.

2.2. Characterization techniques of the photocatalytic nanocomposite

Crystal structure of the photocatalytic nanoparticles was characterized by X-ray diffraction (XRD) patterns using a Rigaku D-max C III, X-ray diffractometer with Ni-filtered Kα radiation (λ=1.5418 Å). Scanning electron microscopy (SEM) (Philips XL 30) was used to assess the morphology of the synthesized photocatalyst. The UV–vis diffuse reflectance spectra (DRS) were achieved using a UV–Vis spectrophotometer (Shimadzu 1800). The zeta potential analysis (JS94H) was performed at various pH values of 3-13.

2.3. Membranes preparation

The bare nanofiltration membrane (M1) was fabricated via the phase inversion caused by the immersion precipitation technique by polyethersulfone basic polymer (PES Ultrason E 6020P, M_w=58 KDa), Poly (N-vinyl pyrrolidone) (PVP, M_w=29 KDa) as pore maker, and N, N-dimethyl acetamide solvent (DMAc, Merck-Germany) based on the literature. To prepare the UV-grafted deposited membranes, the bare membrane was submerged in various concentrations of 0.01, 0.03, and 0.05 wt. % of LTW suspensions at room temperature for 15 min under continuous stirring on a magnetic stirrer at the rate of 200 rpm. The suspensions were provided by adding a sufficient concentration of photocatalyst in distilled water under ultrasonication for 20 min. Afterward, the membranes completely were washed with distilled water and illuminated by 150 W UV lamp from the distance of 20 cm for 15 min. Membranes were named M_2, M_3, and M_4, respectively.

2.4. Characterization techniques of prepared membranes

The Attenuated Total Reflection-Fourier Transforms Infrared (ATR-FTIR) spectroscopy is recorded by Bruker spectrometer (TENSOR 27) to probe the surface chemistry of membranes. Scanning electron microscopy (SEM) instrument (Philips-X130 and Cambridge scanning electron microscope) was utilized to study the fabricated membrane surface and its cross-sectional morphologies. For cross-sectional image, the membranes' samples before broken were frozen in a liquid nitrogen bath. The roughness of the membranes' surface was analyzed by Atomic force microscopy (AFM) analysis. To characterize the membranes surface topography, the roughness parameters i.e., the mean roughness (R_a), the root mean square of the Z data (R_q) and the mean difference between the highest peaks and the lowest valleys (R_y) were assembled and analyzed by Nanosurf C3000 software. Also, the static water contact angle (WCA) was measured using a goniometer (G10, KRUSS, Germany) to assess surface hydrophilicity of fabricated membranes. In this regard, 2 µl of distilled water is dropped at five random points on the membrane surface for each of the membranes.

2.5. Filtration experiments

The filtration performance and antifouling properties of fabricated photocatalytic membranes were studied by a dead-end setup with an effective membrane area of 19.625 cm2 and a volume capacity of 250 ml. Prior to measurement of the pure water flux (PWF), the membranes were soaked in distilled water for 30 min and then were installed in the cell. Once the membranes were pre-compacted for 30 min at 5 bar, then the working pressure was lowed to 4 bar. During nanofiltration, the permeate samples were collected and weighed every 5 min. The PWF (Jw.1) was calculated according to following equation:

$$J_w = \frac{M}{A.\Delta t} \quad (1)$$

where, M, A, and Δt denote the mass of permeated water (kg), membrane effective area (m^2), and permeation duration (h), respectively (Zangeneh et al. 2019a).

The antifouling property of the prepared membranes was assessed by a milk powder solution with a concentration of 1000 mg/l as a foulant. To this end, the milk powder solution was filtered for 1.5 h, at pressure of 4 bar and the permeate flux (J_p) was measured. Afterwards, the used membrane was washed and rested in distilled water for 30 min to recovery. The filtration process was continued by passing distilled water for further 1.5 h, and second pure water flux ($J_{w.2}$) was measured. The flux recovery ratio (FRR), reversible fouling ratio (R_r), and irreversible fouling ratio (R_{ir}) of the fabricated membranes were calculated by the equations below (Zinadini et al. 2014; Oulad et al. 2020):

$$FRR\ (\%) = \left(\frac{J_{w.2}}{J_{w.1}}\right)\times 100 \quad (2)$$

$$R_r = \left(\frac{J_{w.2}-J_p}{J_{w.1}}\right)\times 100 \quad (3)$$

$$R_{ir} = \left(\frac{J_{w.1}-J_{w.2}}{J_{w.1}}\right)\times 100 \quad (4)$$

2.6. Self-cleaning performance of membranes

Methyl red (MR) dye as the azo dye in industrial wastewater was filtered to assess the self-cleaning property of membranes out through a plexiglass dead-end filter system equipped with a LED lamp. The self-cleaning experiments were carried over three steps of 1 h from dark condition, under visible light irradiation, to the dark condition. In such a way that, 50 mg/L MR dye solution was filtered under the dark condition for 1 h at 4 bar. Then, the membrane was irradiated by a 50 W LED lamp for 1 h. The MR dye was passed through the membrane under the aforementioned condition again. In each step, sampling was conducted every 10 min to the measurement of flux and dye removal in order to compare them before and after light irradiation. Self-cleaning property due to the membrane's photoactivity was illustrated by comparing flux and also dye removal. The dye removal efficiency (R (%)) was determined via measure dye concentrations in permeate (C_p) and feed (C_f) using a UV–vis spectrophotometer at its λ_{max} (516 nm) and subsequently by the following equation:

$$R(\%) = (1-C_p/C_f)\times 100 \quad (5)$$

Furthermore, after selecting the optimal membrane (M_3, accordingly to prior experiments result), the long-term filtration was conducted using MR dye under visible light irradiation and also dark conditions at 4 bar for 12 h. The permeation flux was measured every 30 min.

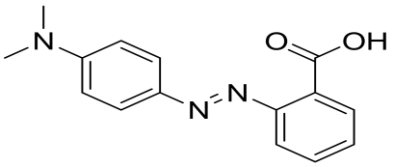

Fig. 1. Chemical structure of MR dye molecule.

Fig. 2. Photograph of the dead-end set-up under light irradiation and dark condition.

3. Results and discussion

3.1. Characterization of the prepared photocatalyst

The crystalline phase structure of the pure TiO_2 and L-lysine codoped TiO_2-WO_3 photocatalytic nanocomposite is anatase with diffraction peaks at 2θ= 25.1°, 37.8°, 48.1°, 53.9°, 55.0°, 62.5°, 68.8°, 70.5°, 75.5° correspond to (101), (004), (200), (105), (211), (204), (116), (220), (215) planes, respectively (Fig. 3a) (Zangeneh et al. 2020). The surface morphology of photocatalytic nanocomposite was investigated using SEM images (Fig. 3b). From Fig. 3b, the photocatalyst nanoparticles have a uniform and spherical shape. The particle size distribution in the 20–40 nm range was obtained using the analysis software of NIH Image J on the SEM images of the surface morphology. The light absorption properties of the photocatalytic nanocomposite were determined using UV–vis DRS spectra and Tauc plots (Fig. 3c, d). The prepared photocatalyst had a significant light absorption into the visible light region. Also, the energy gap reduction of the LTW composites is shown in Fig. 3d, which is 2.1 eV vs. 3.2 eV for the anatase TiO_2. This difference is owing to a red shift into the visible region that leads to photo-exciting of the composite surface electrons by photons with lower energy, resulting in increasing of photocatalytic activity. This reduction in band gap energy was ascribed to WO_3 nanoparticles as a sensitizer as well as the creation of additional energy level by L-Lysine as a dopant agent between CB and VB of pure TiO_2 (Rafiee et al. 2018).

3.2. Physicochemical properties of membranes

Fig. 4 depicts the ATR-FTIR spectrum of the bare membrane (M_1) and selected modified membrane (M_3) to inspect the surface chemistry. The bare PES membrane (M_1) displays characteristic peaks at 1105, 1244, 1485, 1578, 1151, and 1322 cm^{-1}, which is attributable to the C-O stretching, aromatic ether stretching, aromatic nature or C=C stretching, benzene ring stretching, and the symmetric and asymmetric O=S=O stretching, respectively (Zangeneh et al. 2022). As can be seen, the characteristic absorption bands of the M_3 membrane's spectrum include all aforementioned peaks which indicate the absence of polymer degradation under UV irradiation.

However, the different absorbance intensities can be seen in the range 800-1155 cm^{-1} which may be due to the hydrogen bonds between nanophotocatalyst and basic polymer and or oxygen atoms of –COOH, –SO_2OH, and ether groups of the PES polymer (Kovács 2017). Furthermore, the peak at 760 cm^{-1} is responsible for tensile vibration of the Ti-O and Ti-O-Ti bond.

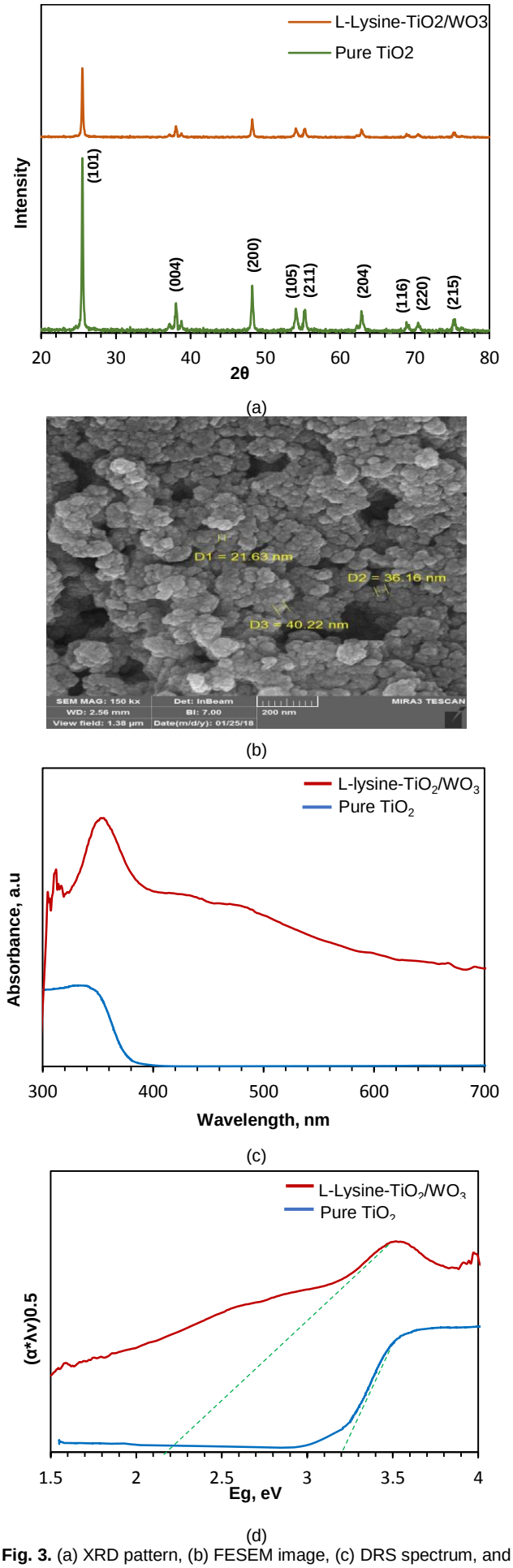

Fig. 3. (a) XRD pattern, (b) FESEM image, (c) DRS spectrum, and (d) Tauc plot of photocatalytic nanocomposite.

The three stronger peaks of 1151, 837, and 868 cm^{-1} related to bending and stretching vibrations of the TiO_2 and WO_3 confirm the successful synthesis of photocatalytic membranes (Madaeni et al. 2011).

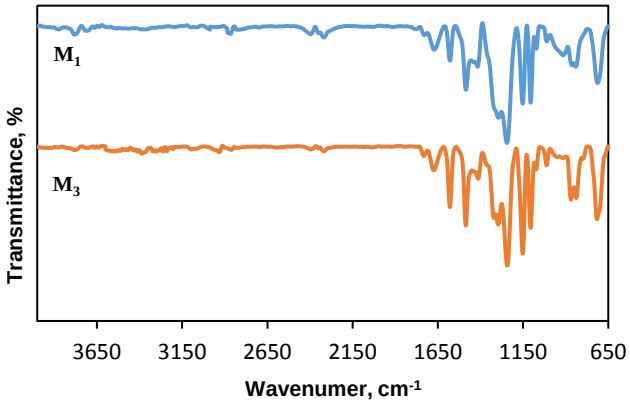

Fig. 4. FT-IR spectra of the bare and modified membranes.

Fig. 5 shows the FE–SEM images of top–surface and cross–section, and three-dimensional (3D) AFM images of the prepared membranes. The cross–sectional image of the modified membranes represents no substantial alteration to the bare membrane. The M_2 and M_3 SEM images of the top–surface show a smooth surface without any aggregation of the nanocomposite. This confirmed by AFM analysis. As seen in AFM results in Fig. 6 and Table 1, these modified membranes have a smoother surface than bare membrane. According to the literature, alleviation of surface roughness is associated to the formation of a photocatalytic layer on the modified membranes' surface. While, increased amount of photocatalytic nanocomposite (M_4) on the membrane surface lead to aggregation and surface roughness and subsequently obstruction of the membrane surface pores and also further fouling (Salehian et al. 2022; Jorge et al. 2014).

Table 1. Roughness parameters of the prepared membranes.

Membrane	R_a, nm	R_q, nm	R_z, nm
M_1	45.21±0.9	61.38±1.22	436.72±8.73
M_2	8.83±0.18	10.55±0.21	51.74±1.03
M_3	1.34±0.02	3.54±0.07	8.62±0.17
M_4	4.15±0.83	5.37±0.1	28.44±0.57

Since an evaluation index of hydrophilicity is the water contact angle (WCA), the result of WCA measurement for prepared membranes is indicated in Fig. 6 (Russo et al. 2021). The WCA values of 63.4, 49.5, 42.6, and 40.2° resulted for M_1, M_2, M_3, and M_4 membranes, respectively. Increasing the amount of photocatalyst coated on the membrane's surface cause further hydrophilicity, consequently improving the hydrophilicity and performance of the membrane's surface.

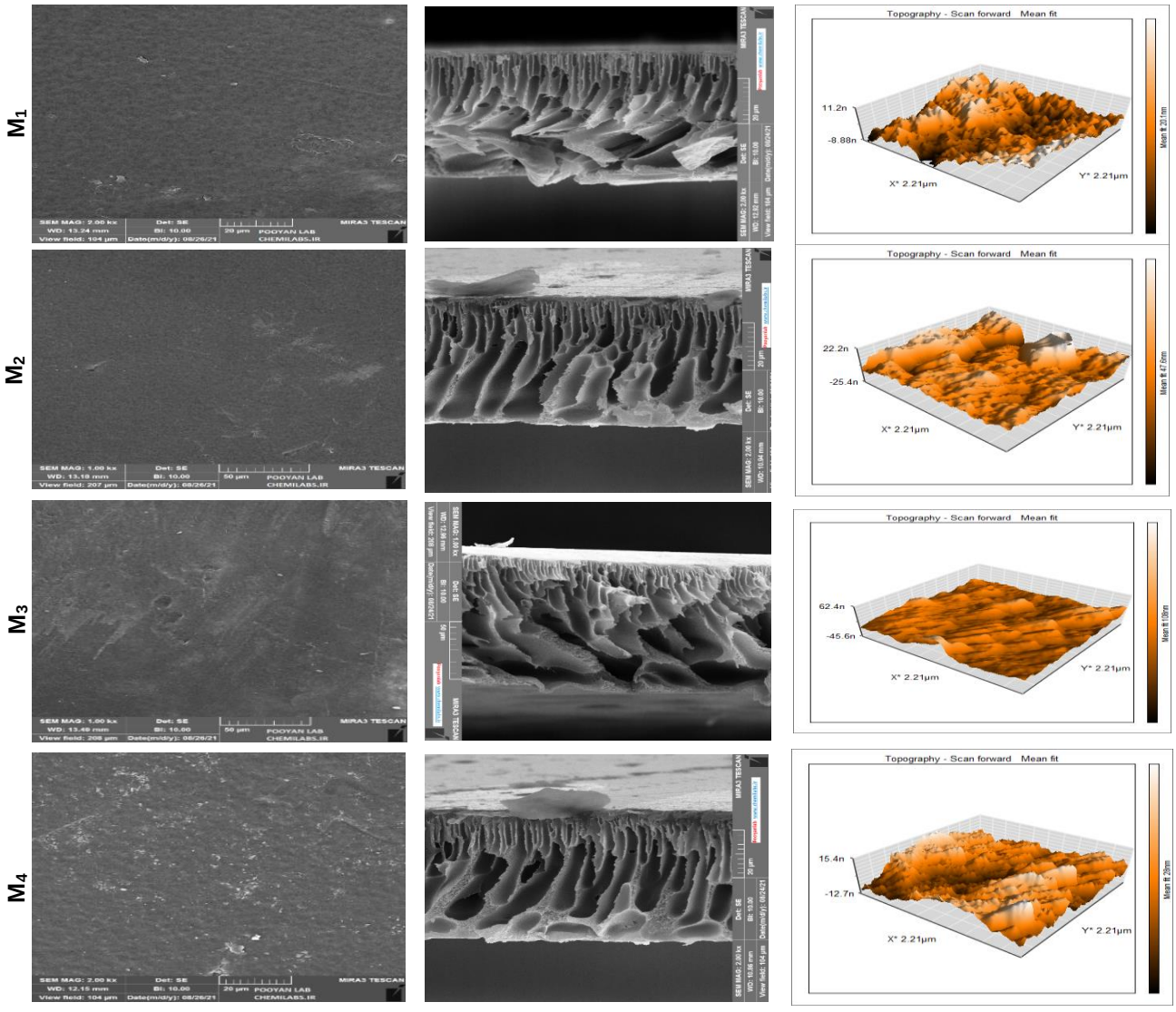

Fig. 5. The surface and cross–section FE–SEM images and AFM analysis of the fabricated membranes.

It is clear that an increase in membrane surface hydrophilicity leads to easier passage of water molecules and as a result the enhancement of permeation flux (Khemakhem et al. 2020). In this direction, the pure water flux (PWF) of the prepared membranes also is displayed in Fig. 7. As can be seen, the photocatalytic membranes had higher PWF than the unmodified membrane. From Fig. 7, PWF showed a variation trend

consistent with hydrophilicity. However, when the nanophotocatalyst content ascends, the PWF reduces due to the agglomeration phenomenon (as shown in SEM image, Fig. 5).

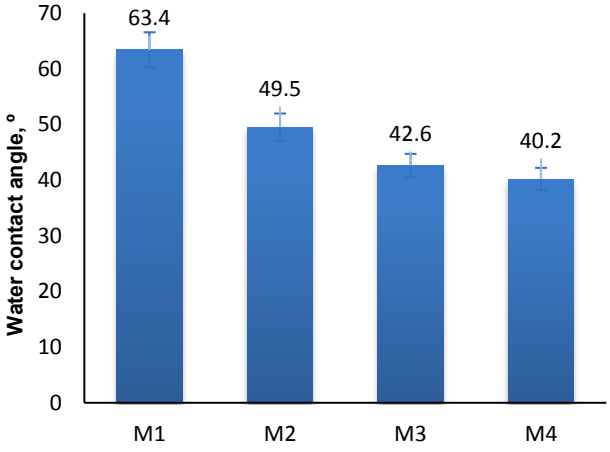

Fig. 6. Water contact angle of the membranes.

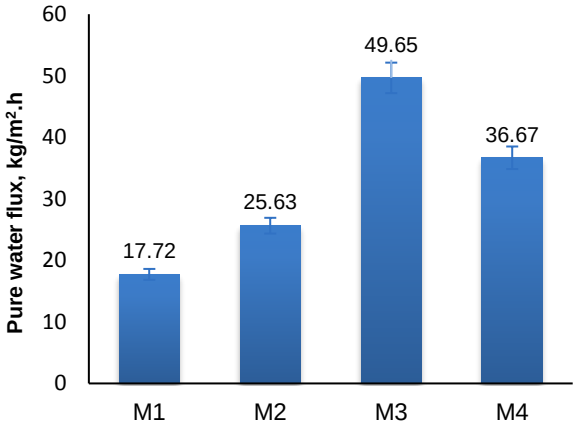

Fig. 7. Pure water flux of the prepared membranes.

3.3. Antifouling performance of membranes

The antifouling properties of fabricated membrane were evaluated via measurement of flux recovery ratio (FRR, %) and fouling parameters (R_r (%) and R_{ir} (%)) values by nanofiltration of 1000 ppm milk powder solution using dead end set up (T. Wu et al. 2019). The FRR, R_r, and R_{ir} values as well as PWF and WCA of the photocatalytic membranes are depicted in Table 2 to provide a comprehensive comparison of all prepared membranes. As can be seen, the FRR values were increased to 96.96% for the M_3 membrane in contrast to 54.57 % for the bare membrane. In order to further evaluation of the membranes' antifouling behavior, the fouling resistance parameters i.e., R_r and R_{ir} were verified. The results indicative higher R_r and less R_{ir} for modified membranes compared to unmodified membrane. The TiO_2-based photocatalyst on the membranes' surface not only leads to high hydrophilicity (WCA result) through adsorption of the water layers but also by formation smoother surface (AFM image) hinders from further fouling formation (Salazar et al. 2020). Totally, all photocatalytic membranes revealed amelioration of filtration performance and antifouling properties. It is worth noting among modified membranes, the M_3 membrane with having excellent antifouling properties (R_r 64.25% and R_{ir} 3.69 %) and high nanofiltration (PWF 49.65 vs. 17.72 kg/m^2.h for bare membrane) has promising performance for real wastewater treatment.

Table 2. The results of membrane performance.

	PWF, kg/m^2.h	WCA, °	FRR, %	R_r, %	R_{ir}, %
M_1	17.72±0.3	63.4±1.2	54.57±1.09	36±0.72	45.42±0.90
M_2	25.63±0.5	49.5±0.9	84.65±1.6	49.64±0.99	15.34±0.30
M_3	49.65±0.9	42.6±0.8	96.96±1.93	65.04±1.30	3.03±0.06
M_4	36.67±0.7	40.2±0.8	90.51±1.81	59.53±1.19	9.48±0.18

3.4. Photocatalytic capability of membranes

The efficacy of light irradiation on the flux for prepared membranes was shown in Fig. 8. The flux mitigation was observed for all of the membranes before and after light irradiation. However, after visible light irradiation, despite the decreasing trend of the flux for bare membrane, the photocatalytic membranes' flux indicated an increasing trend. Although, a decreasing trend was observed for the photocatalytic membranes in the continuation of the filtration, but was less downward trend compared to the filtration before the light irradiation.

In order to assessment of the membranes' photoactivity, the dye removal for all membranes before and after light irradiation was shown in Fig. 9. As can be seen, the dye removal of the bare membrane indicated no difference before and after visible light irradiation. However, the modified membranes had a higher dye removal after visible light irradiation than primary dark condition (94.36 vs. 86.55 % for M_3 membrane).

The presence of photocatalytic nanocomposite on a modified membrane creates the superhydrophilicity feature under visible light irradiation. The light irradiation through reducing Ti (IV) cations to the Ti (III) state and oxidizing O^{2-} anions of the nanocomposite lead to the occupation of empty sites of oxygen by the water molecules and adsorption of the water layers (Ngo et al. 2020; Rahimpour et al. 2008). Furthermore, the production of the electron and hole pairs due to light irradiation to photocatalytic nanocomposite lead to photoactivity of photocatalytic membranes and subsequently flux and dye removal enhancement via mitigation of membrane fouling and surface polarization (Hoseini et al. 2017).

Among modified membranes, the M_3 membrane with having high PWF, excellent antifouling, and self-cleaning property as a result of high hydrophilicity (WCA result), smoother surface (AFM result), and the improved photoactivity (dye removal result) was selected as optimal membrane for further examination.

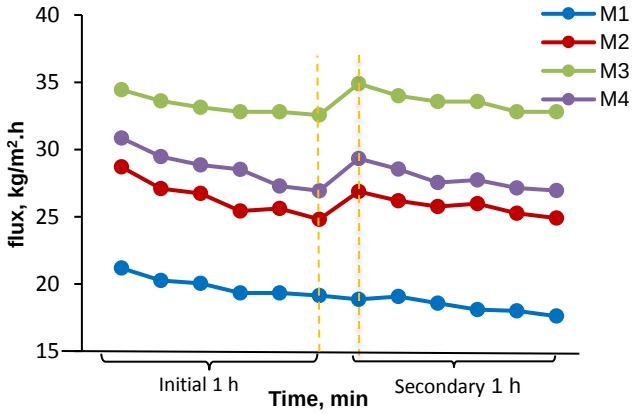

Fig. 8. The permeation flux of the fabricated membranes before and after visible light irradiation.

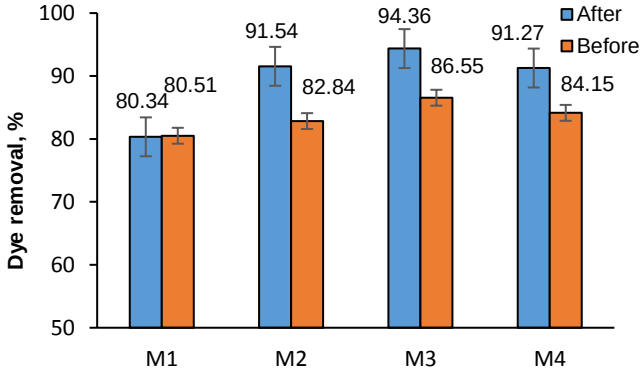

Fig. 9. The dye removal of the fabricated membranes before and after visible light irradiation.

The long-term filtration process was also conducted for the M_3 membrane at 4 bar for 12 h under visible light irradiation and the dark condition. From Fig. 10, the M_3 membrane's flux under visible light has remained stable from 34.51 to 30.61 kg/m^2.h, whereas that of dark condition has progressively decreased from 33.74 to 19.6 kg/m^2.h. The great antifouling behavior and permeation stability of the optimal membrane (M_3) provided under visible light irradiation be attributed to superhydrophilic and photoactivity of the nanocomposite on the membrane surface.

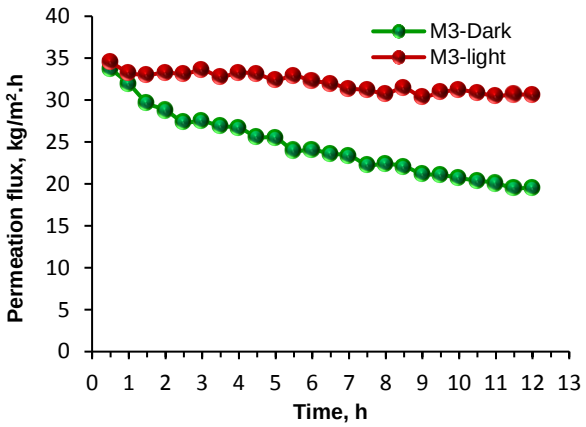

Fig. 10. Long-term filtration performance of the M_3 membrane under visible light irradiation and dark condition.

4. Conclusions

In this work, a TiO_2-based photocatalyst was successfully used as a surface modifier for the PES nanocomposite membrane. The surface morphology, roughness, hydrophilicity, permeability, antifouling properties, and photoactivity of the photocatalytic membranes were affected by the weight percent of photocatalytic nanocomposite grafted on the membrane surface. Among fabricated membranes, M_3 membrane due to having optimum performance characteristics i.e., high hydrophilicity (WCA of 42.6 vs. 63.4° for bare membrane), antifouling properties (FRR of 96.96 vs. 57.57% for bare membrane), and photoactivity (dye removal of 94.36 vs. 80.34 % dye removal for bare membrane) was chosen as the desirable membrane. The long-term filtration capacity of the optimum photocatalytic membrane (M_3) was assessed under visible light irradiation than dark conditions. The results represented a great long-term and photoactivity performance under visible light irradiation.

Acknowledgment

The authors would like to acknowledge Iran Nanotechnology Innovation Council (INIC) for the financial support provided for this research work. The authors also wish to thank Razi University-Iran for the equipped lab.

Nomenclature

PES	polyethersulfone
LTW	C, N codoped-TiO_2/WO_3
WCA	water contact angle
PWF	pure water flux
CQDs	carbon quantum dots
XRD	X-ray diffraction
SEM	Scanning electron microscopy
DRS	UV–vis diffuse reflectance spectra
ATR-FTIR	Attenuated total reflection fourier transforms infrared
AFM	Atomic force microscopy
R_a	Mean roughness
R_q	Root mean square of the Z data
R_y	Difference between highest peaks and lowest valleys
FRR	Flux recovery ratio
R_r	Reversible fouling ratio
R_{ir}	Irreversible fouling ratio
MR	Methyl red
R	removal efficiency
3D	three-dimensional

References

Aboamera N.M., Mohamed A., Salama A., Osman T. A., Khattab A,. An effective removal of organic dyes using surface functionalized cellulose acetate/graphene oxide composite nanofibers, Cellulose 25 (2018) 4155–4166.

Basumatary B., Basumatary R., Ramchiary A., Konwar D., Evaluation of Ag@TiO_2/WO_3 heterojunction photocatalyst for enhanced photocatalytic activity towards methylene blue degradation, Chemosphere 286 (2022) 131848.

Chiao Y.H, Chen S.T., Sivakumar M., Ang M., Patra T., Almodovar J., Wickramasinghe S., Hung W., Lai J., Zwitterionic polymer brush grafted on polyvinylidene difluoride membrane promoting enhanced ultrafiltration performance with augmented antifouling property, Polymers 12 (2020) 1–12.

Chi L., Qian Y., Guo J., Wang X., Arandiyan H., Jiang Z., Novel G-C_3N_4/TiO_2/PAA/ PTFE ultrafiltration membrane enabling enhanced antifouling and exceptional visible-light photocatalytic self-cleaning, Catalysis Today 25 (2019) 4155-4166.

Garcia-Ivars J., Iborra-Clar M.I., Alcaina-Miranda M.I., Mendoza-Roca J.A., Pastor-Alcañiz L., Development of fouling-resistant polyethersulfone ultrafiltration membranes via surface uv photografting with polyethylene Glycol/Aluminum oxide nanoparticles, Separation and Purification Technology 135 (2014) 88–99.

Heng Z.W., Chong W.C., Pang Y.L., Koo C.H., Self-Assembling of NCQDs-TiO_2 nanocomposite on poly(acrylic acid)- grafted polyethersulfone membrane for photocatalytic removal and membrane filtration, Materials Today: Proceedings 46 (2021) 1901-7.

Hoseini S.N., Pirzaman A.K, Aroon M.A., Pirbazari A., Photocatalytic degradation of 2,4-Dichlorophenol by co-Doped TiO_2 (Co/TiO_2) nanoparticles and Co/TiO_2 containing mixed matrix membranes, Journal of Water Process Engineering 17 (2017) 124–34.

Khemakhem A., Ben Romdhane M.R., Srasra E., Improved performance of ultrafiltration membranes after surface modification, Surface Engineering and Applied Electrochemistry 56 (2020) 561–570.

Kovács I., Veréb G., Kertész S., Hodúr C., László Z., Fouling mitigation and cleanability of TiO_2 photocatalyst-modified PVDF membranes during ultrafiltration of model oily wastewater with different salt contents, Environmental Science and Pollution Research 25 (2017) 34912-34921.

Madaeni S.S., Zinadini S., Vatanpour V., A new approach to improve antifouling property of pvdf membrane using in situ polymerization of PAA functionalized TiO_2 nanoparticles, Journal of Membrane Science 380 (2011) 155–162.

Mansourpanah Y., Shahebrahimi H., Kolvari E., PEG-Modified GO nanosheets, a desired additiveto increase the rejection and antifoulingcharacteristics of polyamide thin layer membranes, Chemical Engineering Research and Design 104 (2015) 530–540.

Ngo T.H.A., Nguyen C.T.M., Do K.D., Duong Q.X., Tran D.T., Nguyen H.T., Tran N.H., Improvement of hydrophilicity for polyamide composite membrane by incorporation of graphene oxide-titanium dioxide nanoparticles, Journal of Analytical Methods in Chemistry (2020).

Oulad F., Zinadini S., Zinatizadeh A.A., Derakhshan A.A., Preparation and characterization of loose antifouling nanofiltration membrane using branched aniline oligomers grafted onto polyether sulfone and application for real algal dye removal, Chemical Engineering Journal 401 (2021) 125861.

Pejman M., Firouzjaei M., Aghapour S., Zolghadr E., Das P., Elliott M., Sadrzadeh M., Sangermano M., Rahimpour A., Tiraferri A., Effective strategy for uv-mediated grafting of biocidal ag-mofs on polymeric membranes aimed at enhanced water ultrafiltration, Chemical Engineering Journal 426 (2021) 935-945.

Rafiee E., Noori E., Zinatizadeh A.A., Zangeneh H., A new visible driven nanocomposite including Ti-substituted polyoxometalate/TiO_2 :synthesis,characterization,photodegradation of Azo dye process optimization by RSM and specific removal rate calculations, Journal of Materials Science: Materials in Electronics 29 (2018) 20668–20679 .

Rahimi Z., Zinatizadeh A.A., Zinadini S., Loosdrecht M.V., A hydrophilic and antifouling nanofiltration membrane modified by citric acid functionalized tannic acid (CA-f-TA) nanocomposite for dye removal from biologically treated baker's yeast wastewater, Journal of Environmental Chemical Engineering 9 (2021) 104963.

Rahimpour A., Madaeni S.S., Taheri A.H., Mansourpanah Y., Coupling TiO_2 nanoparticles with UV irradiation for modification of polyethersulfone ultrafiltration membranes, Journal of Membrane Science 313 (2008) 158–69.

Russo F., Bulzomì M., Nicolò E., Ursino C., Figoli A., Enhanced anti-fouling behavior and performance of pes membrane by UV treatment,

Processes 9 (2021) 1–17.

Salazar H., Martins P.M., Santos B., Fernandes M.M., Reizabal A., Sebastián V., Botelho G., Tavares C.J., Vilas-Vilela J.L., Lanceros-Mendez S., Photocatalytic and antimicrobial multifunctional nanocomposite membranes for emerging pollutants water treatment applications, Chemosphere 250 (2020) 126299.

Salehian S., Heydari H., Khansanami M., Vatanpour V., Mousavi S.A., Fabrication and performance of polysulfone/H_2O_2-g-C_3N_4 mixed matrix membrane in a photocatalytic membrane reactor under visible light irradiation for removal of natural organic matter, Separation and Purification Technology 285 (2022) 120291.

Wu L., Zhang X., Wang T., Du Ch., Yang C., Enhanced performance of polyvinylidene fluoride ultrafiltration membranes by incorporating TiO_2/Graphene oxide, Chemical Engineering Research and Design 141 (2018) 492-501.

Wu T., Zhang Z., Zhai D., Liu Y., Liu Q., Xue L., Gao C., Dye degrading and fouling-resistant membranes formed by deposition with ternary nanocomposites of N-Doped graphene/TiO_2/ activated carbon, Membranes 9 (2019) 9010016.

Xia W., Xie M., Feng X., Chen L., Zhao Y., Surface modification of poly(vinylidene fluoride) ultrafiltration membranes with chitosan for anti-fouling and antibacterial performance, Macromolecular Research 26 (2018) 1225-1232.

Zabihi Z., Homayoonfal M., Davar F., Application of UV Irradiation enhanced by CuS photosensitive nanoparticles to mitigate polysulfone membrane fouling, Journal of Photochemistry and Photobiology A: Chemistry 390 (2020) 112304.

Zangeneh H., Zinatizadeh A.A., Zinadini S., Feyzi M., Bahnemann D., Preparation and characterization of a novel photocatalytic self-cleaning pes nanofiltration membrane by embedding a visible-driven photocatalyst Boron Doped-TiO_2–SiO_2/$CoFe_2O_4$ nanoparticles, Separation and Purification Technology 209 (2019) 764–775.

Zangeneh H., Zinatizadeh A.A., Zinadini S., Preparation ultrafine L-methionine (C,N,S Triple Doped)-TiO_2-ZnO nanoparticles and their photocatalytic performance for fouling alleviation in PES nanocomposite membrane, Composites Part B: Engineering 176 (2019) 107158.

Zangeneh H., Zinatizadeh A.A., Zinadini S., Self-cleaning properties of L-Histidine doped TiO_2-CdS/PES nanocomposite membrane: Fabrication, characterization and performance, Separation and Purification Technology 240 (2020) 116591.

Zangeneh H., Mousavi S.A., Eskandari P., Comparison the visible photocatalytic activity and kinetic performance of amino acids (non-metal doped) TiO_2 for degradation of colored wastewater effluent, Materials Science in Semiconductor Processing 140 (2022) 106383.

Zinadini S., Zinatizadeh A.A., Rahimi M., Vatanpour V., Preparation of a novel antifouling mixed matrix pes membrane by embedding graphene oxide nanoplates, Journal of Membrane Science 453 (2014) 292–301.

Zou H., Ren X., Zhang J., Fabrication of a Bi_2O_3 surface-modified polyvinylidene fluoride membrane via an ultraviolet photografting method: improving hydrophilicity and degree of acrylic acid grafting, Industrial & Engineering Chemistry Research 59 (2020) 6580-6588.